Impact of surface roughness on energy harvesting: Comparative study of smooth and rough cylinder.

Author

Muhammad Hammad Bucha

Registration Number

2019-NUST-MSME-00000319612

Supervisor

Dr. Niaz Bahadur Khan

DEPARTMENT OF MECHANICAL ENGINEERING

SCHOOL OF MECHANICAL & MANUFACTURING ENGINEERING

NATIONAL UNIVERSITY OF SCIENCES AND TECHNOLOGY

ISLAMABAD

December 2021

Copyright Statement

Acknowledgements

I am thankful to my Creator Allah (SWT) to have guided me throughout this work at every step and for every new thought which you setup in my mind to improve it. Indeed, I could have done nothing without Your priceless help and guidance. Whosoever helped me throughout the course of my thesis, whether my parents or any other individual was Your will, so no doubt none be worthy of praise but You.

I am profusely thankful to my beloved parents who raised me when I was not capable of walking and continued to support me throughout in every department of my life.

I would also like to express special thanks to my supervisor Dr. Niaz Bahadur Khan for his help throughout my thesis.

I would also like to pay special thanks to Dr. Emad uddin for his tremendous support and cooperation. Each time I got stuck in something, he came up with the solution. Without his help I wouldn't have been able to complete my thesis. I appreciate his patience and guidance throughout the whole thesis.

I would also like to thank Dr. Adnan Munir, Dr. Muhammad Sajid and Dr. Waqas Khalid for being on my thesis guidance and evaluation committee and express my special gratitude to me for my help throughout the project.

Finally, I would like to express my gratitude to all the individuals who have rendered valuable assistance to my study.

Dedicated to my parents, mentors, and loving siblings whose untiring effort and dedication which boosted me to this wonderful novelty.

Table of Contents

List of Figures

Impact of surface roughness on energy harvesting: Comparative study of smooth and rough cylinder.

Abstract

The world is moving towards renewable energy resources as an efficient way of energy harvesting because of the depleting energy resources and the low installation cost. One of the sources of energy harvesting is the hydel source which takes advantage of the flow energy of water in oceans to generate energy. This experimental study aims to investigate the effect of surface roughness of cylindrical cylinders on the energy harvested by piezoelectric eels using low-speed water tunnels. The piezoelectric eel is placed in the wake of the cylinders with varying roughness. The experiments are performed for four different roughness (K_s/D) of 8.8 $x10^{-5}$, 1.51 x 10^{-4}, 3.62 x 10^{-4} and 5.08 x 10^{-4} of the cylinder. For each roughness, the distance between the center of the cylinder and the center of the eel is changed both in x- and y-direction. The flapping frequency, dimensionless amplitude, and optimal power of the rough cylinders are analyzed and compared with that of the smooth cylinder. The highest power is obtained on the eel at the optimal point. By increasing the surface roughness of the bluff body, the lock-in region decreases and as a result, the harvested power from that bluff body wake is reduced. Moreover, the power also decreases with increasing the distance between the cylinder and eel both in x- and y-direction.

Chapter 1

Introduction

1.1 Green Energy resources

Novel technologies and advanced materials are replacing the conventional methods to harvest energy from natural resources. One such technology is the use of the piezoelectric effect to generate electricity from flowing fluid obstructed by a simple bluff body. The bluff body induces vortices in the flow which cause stress in a piezoelectric material usually in the shape of thin, flexible, piezoelectric membranes and it is used to harvest electrical energy, was studied by Leland et al. [1] and Kamenar, E et al. [2]. Eels placed in the flow domains of rivers, streams, and oceans can extract energy to power small systems without severely damaging the ecosystem. Eels placed axially in the direction of flow generate energy by flapping caused by the solid interaction with bluff body-induced vortices was studied by Xie[1], J et al [3].

1.2 Sub- Sea energy harvesting

Energy harvesting using piezoelectric eels has many modern low-input power applications. Underwater microelectromechanical devices used as sensors and actuators, especially in offshore oil and gas extraction sites, can be made self-sufficient with the use of this technology is studied by Williams, C. B et al [4]. The amount of energy extracted is dependent upon the strength of vortices induced in the flow which, in turn, is dependent upon the shape of the bluff body, and it is surface roughness is studied by Wang, Q et al [5].

1.3 Piezo electricity

PVDF's piezoelectric activity is examined in this article, as well as some of its possible uses. There are four crystal types of PVDF semicrystalline polymer. These shapes can be altered using heat, electromagnetism, and pressure. To keep the eddy currents in the crystallized areas, we'll utilize thermal or corona poling. crystal and amorphous parts of polyvinylidene fluoride (PVDF) provide it unique dielectric and elastic properties. The piezoelectric constant d31 reaches 35 p C/N at room temperature. Temperature has a negative effect on the D31 and D33 values. PVDF's low electromechanical coupling factor offers it an advantage over other materials, making it flexible, long-lasting, and capable of forming thin layers. piezoelectric ceramic devices, ultrasound transducers, and immersed transducers all use this technology.

1.4 Piezo electric effect

Hemispherical or semi-symmetrical crystals, which have axis with opposing poles, have two conflicting electric poles as the temperature varies. Pyroelectricity or pyroelectricity is the scientific term for this phenomenon. The piezoelectric effect was studied using bones that were depleted of minerals or collagen. Bone's piezoelectric activity may be due in part or in total to its organic components, according to these studies. Both outcomes can occur if the collagen-mineral interaction is misunderstood. Mineral composition has no effect on bone's piezoelectric activity.

Figure 1.1 Piezoelectric eel

Allen, Jet al. [8]. Figure 1.1 shows a piezoelectric eel connected on one end with metal support and an electrical connection. In such a configuration the eel's flapping resembles the vibration of a cantilever beam. The flapping area of the eel has a wide role in sense of result outputs.

1.5 Experimental Parameters

The area of interest eel is compared in sense of S/D, L/D ratio also the dynamic variation of Reynolds number. To plot the variation in the results diversity of experimental data sets is arranged according to a different diameter. The speed of flowing water is also varied to collect different data set. Sub-critical points and post-critical points are also to be pondered for fine results. As in upstream flow, the moving towards the flow the energy harvested is increased as

the flapping increases and energy harnessing is effective. As the S/D ratio is increased from 1 to 2 the considerable change in voltage is visible when S/D is increasing to 3 then vortex shedding is dropped causing a decrease in voltage. Higher energy gained at the points was discussed at the optimum distance and speed U, the maximum energy to be harnessed. A significant increase in energy is observed which is 38% is discussed by Uddin, E et al. [9]

Chapter 2

Literature Review

A lot of work has been done on cylindrical bluff bodies either full or cut, square bodies is studied by Rocha, J et al [6]. However, very little research work is available on the effect of bluff body aging on the energy harvested from the eel. This work investigates this parameter by varying the surface roughness of the cylindrical bluff body and finding the optimum location at which the harvested energy is maximum is studied by Simpson, R. L [7]. The age of bluff body after which energy harvested drops to a certain minimum level after that roughness of the bluff body is replaced.

2.1 Wind tunnel experimental analysis

Okaijima. A et al. [18] Experimentally studied the range of Reynold number $2.5x10^4 – 3.2x10^5$ and roughness of range $5x10^{-3} – 3.8\ x10^{-2}$ to verify the impact briefly the experiments were carried out. A free oscillation test was carried out in the wind tunnel. Critical velocity is included in the range of reduced velocity of 1.5 to 8 The amount of reducing mass damping constant at 6. At Reynold's number higher than the critical point a rougher cylinder vibrated with large amplitude. The rough cylinder generates more vibrations as a result chaotic flow is formed which is more vulnerable to dissipate. Vortices are weak and immediately shredded off.

2.2 Rectangular shaped bluff body

Its value ranges from 3200 to 12,000 points. When a circular cylinder is suspended in the wake of a polyethylene terephthalate membrane, flailing and strain energy distribution are changed. A cantilever-like oscillation (mode A) occurs between Reynolds numbers 4000 and 6800, resulting in Mode A response and limited travelling waves (i.e., Mode B). Between Rs. 6,800 and Rs. 12,000, there is a quasi-periodic flapping (i.e., Mode C). When Mode C "locks-in" to the wake vortex-shedding frequency, the ideal flapping frequency is reached. We're using mode C in this scenario. The Reynolds number increases the flaps' amplitude. Flapping is lessened when the Reynolds number rises.

2.3 Diamond arrangement

As a bonus, schooling fish are better at adapting to a changing environment. It was decided to model flexible body shapes after the schooling hydrodynamics of ocean water. Upstream vortices have a tremendous impact on downstream vortices when they interact with one another. Flexible flags and vortices in a viscous flow were explored using an improved version of the immersed boundary approach. To depict the schooling behavior of fish, triangular and diamond flags were employed. It is possible to modify the stream and spanwise gap lengths, as well as the flag bending coefficient, in order to reduce downstream drag coefficients. By using flexible flags in the upstream and downwind directions, the drag of a ship was adjusted. In this study, the gap distance and bending coefficients of each individual flexible flag were taken into account when studying flexible flag interactions.

2.4 Conical Cylinder bluff body

This seminar will also cover new advancements in the use of forced vibrations. If you're looking for an example, examine the difference between an all-directional responsive piston and a transversely responsive piston. Two circular cylinders in tandem are used as a visual aid to show the relationship between them. There are two factors that contribute to the cylinder's high-amplitude transverse vibration.

2.5 T shaped type bluff body

A piezoelectric cantilever generates electricity by turning fluid movement into electrical energy. Even at modest fluid speeds, flutter is possible because of the T-shaped bimorph cantilever. A wind tunnel prototype of 1006030 mm3 was tested. The contraption was able to run on wind speeds of four meters per second (m/s). Using merely a bimorph cantilever, the current method has been deemed cost-effective.

2.6 D shaped type bluff body

To depict a flag in a homogenous viscous flow, an immersion boundary method (IBM) was employed in conjunction with IBM. The flag was swayed by the vortices generated by the cylinder upstream. To allow the flag to flail, the flag's shape and flow must be carefully considered. When it came to generating energy in this experiment, elements like as the length of Flag A and its bending coefficient all had an impact. The flag can sway in one direction or the other and interact with vortices in both positive and harmful ways at varying frequencies.

2.7 Inverted C type bluff body

When harvesting electrical energy from a homogeneous flow, piezo-flags with variable cut angles can be employed to analyze the behavior of flags in the downstream vortex. It's been shown in trials to have flapping modes that are weakly and optimally connected to the wake flow. The energy output of piezoelectric flags is affected by their streamwise spacing and flow speed. According to the findings, the output power of an inverted C-shaped cylinder with a 120° cut angle was superior to that of a circular cylinder. It doesn't matter what the cylinder or flow velocity is if the wake flow is not connected to the piezoelectric flag. Circular and 60-degree inverted C-shaped cylinders are statistically equal in terms of energy harvesting. An increase in dominant frequency occurs as a result of changes in flapping amplitude and development pace. An increase in energy efficiency may be attributed to improved wake dynamics, according to Particle Image Velocimetry. A 120° cut angle architecture provides a significant benefit over the round cylindrical shape. Adjusting the streamwise spacing, flow velocity, and cut angle of the inverted C-shaped cylinder can gather impinging vortices.

2.8 C type bluff body

Latif U et. al. [10] studied the energy harvested from an inverted C-type cylinder by placing it in the flow region with cut angles of 120, 150, and 180 degrees. The energy obtained increased by up to 38.70%, 46.70%, and 43.40%, respectively, as compared to the full cylinder when the eel is placed off the middle line. The different types of inverted C cylinders generate different types of wakes, and thus, the energy maxima are located at different locations.

2.9 Spring mounted circular cylinder

Ding et al. [11] the oscillations generated by a spring-mounted circular cylinder in a wind tunnel were investigated on a high Reynolds number. The flows close to the critical Reynold number were also identified. The roughness of the cylinder was evenly done by glass-bead minor particles. During the free oscillation test, the velocity get decreases from 5 to 8 at which mass damping was maintained up to 6. Relative low speed of wind is kept close to the critical Reynold number when the surface roughness of the cylinder is used. The negative damping is found too small near the Critical Reynold number which can be damped down by adding up the small structural damping close to the critical Reynold number is verified by [28].

2.10 Varying amplitude and Reynold number of bluff bodies

Allen et. al. [12] studied the induced vortices for cylinders with surface roughness varying from $5.1x10^{-5}$ – $5.8\ x10^{-3}$ mm with Reynolds numbers ranging from $1.8x10^{5}$ – $6.5x10^{5}$. The variation of Reynolds number has a significant impact on the ratio of convective forces to diffusive forces on a rough circular cylinder. The identification of drag and VIV at critical and subcritical points of the flexible cylinder was noted for the circular cylinder as far as 20 diameters upstream. Less VIV will generate less frequency resulting in decreased harvested energy. Along with the Reynold number, another important factor which is roughness factor k_s/D is identified to check the effect of roughness on the bluff body also to make the dimensionless study [29].

2.11 Vortex-Induced Vibration

Bernitsas et al. [13] studied the impact of Reynolds number ranging from $8.0x10^{3}$ – $2.0x10^{5}$ and the roughness of the surface ranging from $1.4x10^{-5}$ – $4.2\ x10^{-3}$. The roughness of the cylindrical bluff body has a vital impact on the VIV behavior in terms of flow transition, separation point, drag, and correlation length. Roughness is co-related to the suppression and compression of VIV by varying the starting, ending, and length of base support. Roughness size is defined in terms of the grit size of the surface of the bluff body [30].

2.12 Effect of roughness on the shear layer in the wake.

Every surface has its grit size. It may be low or high but cannot be zero in practical life. The disturbance which is produced by this bluff body amplifies the vortex frequency and the transition range increased. Consequently, the energy harvested is decreased because of increasing the roughness the shear layer of the wake gets narrower also the vortex formed is dissipated immediately as it is formed. As a result of this frequency, less power is harnessed. The relationship between the roughness factor of the bluff body and the power harnessed is studied. In this research, it is studied that the size of surface roughness is required to achieve the desired effect at a low Reynolds number [31].

2.13 Impact of roughness on lock-in region

Gao, Y.et al. [14]. Numerically studied the VIV response characteristics is studied on the cylindrical body varying the surface roughness. In this research, three different values of

roughness were used. The regions were divided into four regimes 1,2,3,4 while regimes 2 and 3 belong to the lock-in region factors including vortex shedding, lock-in the region, vortex shedding frequency, upper branch, desynchronization zone, and lower branch. Moving towards the increase in roughness factor the VIV response is decreasing trend. The finding of this research as the roughness increases the lock-in region gets narrower. While increasing the Vr the Strouhal number shows an increment, and the drag coefficient shows a downward trend [32].

2.14 Chaotic motion and multiple frequencies

The comparison of results of VIV of a smooth cylinder with a rough cylinder. When Reduced velocity is low in the lock-in region is in the range of chaotic motion and multiple frequencies for a rough cylindrical bluff body are reduced as compared to a smooth cylindrical bluff body. While the low velocity of the lock-in region is high compared with the smooth cylindrical bluff body. The reduced velocity range of a smooth cylindrical bluff body compared with chaotic motion tends to increase [33].

2.15 Studying the vortex shedding

Owing to the behavior of the smooth cylinder, the rough cylinder in the range of low velocity 2S, 2T, and 2P has wake vortex shedding regions. The wake vortex shedding region of a smooth cylinder is different from the rough cylinder, which is due to traversing direction, a phase difference of traverse vibrations, vibration amplitude and lift force. Varying the roughness from the smooth cylinder the rough cylinder also forms the 2P Wake vortex shedding in the low-velocity range. The surface roughness varies from 0.005-0.01, the surface roughness tends to suppress the formation of the wake of 2P vortex shedding due to which the pattern of the wake of the 2S vortex is changed which is discussed by Xiangxi, et al. [15].

2.16 VIV response of the smooth and rough vibrating bluff body

Ghazali et al. [16] Verified the VIV from the different roughness factors of the surface in the experimental study. After keeping in view, the free vibration tests the response of the smooth cylinder is noted at reduced speed. A diversity of roughness was utilized in experimentation. The conclusion of this experiment shows that by the increase in roughness the amplitude

response of the vibrating bluff body decreases, the wake region becomes narrower in the low reduced velocity region.

2.17 Constructive phenomena in frequency

Ramzi, et al. [17] studied by simulating the cylinder with different roughness. As the roughness is high the higher the amplitude reduction was noticed. The vortex-induced vibration is studied in this research and the impact of surface roughness is studied in detail. For a short rigid cylinder, the effect of low reduced velocity is studied by increasing the roughness the lock-in region gets closer and narrower. The amplitude increases when frequency approaches natural frequency which is 1 at low reduced velocity. The constructive phenomena of matching the frequencies give rise to the high frequency and amplitude of the flapping flag.

2.18 Amplitude increment and drag force decrement

K, Y, Kui et al. [19] Studied the range of Reynold number ranging $1.7x10^4$ – $8.3x10^4$ and surface roughness ranging from $2.8x10^{-4}$ – $1.4\ x10^{-2}$ which is uniform roughness of cylinder has reasonable impacts on the hydrodynamic effects of the cylinder. The results of this experimentation show that traverse amplitude tends to decrease as the roughness of the cylinder is decreased as a result narrower wake region is formed. The maximum drag force decreases as the roughness is decreased. The width of the lock in region tends to decrease as the roughness increases.

Research Paper	Reynolds Number	Surface Roughness
Allen, D.W. and Henning, D.L., 2001, April. [20]	$1.8x10^5$ – $6.5x10^5$	$5.1x10^{-5}$ – $5.8\ x10^{-3}$
Bernitsas, M.M., Raghavan, K. and Duchene, G., 2008, January. [21]	$8.0x10^3$ – $2.0x10^5$	$1.4x10^{-5}$ – $4.2\ x10^{-3}$
Kiu, K.Y., Stappenbelt, B. and Thiagarajan, K.P., 2011. [22]	$1.7x10^4$ – $8.3x10^4$	$2.8x10^{-4}$ – $1.4\ x10^{-2}$
Gao, Y., Fu, S., Wang, J., Song, L. and Chen, Y., 2015. [23]	$2.5x10^4$ – $1.8x10^5$	$1.1x10^{-4}$ – $1.2\ x10^{-2}$

Table 1 Reynolds number and surface roughness ranges of past literature work

2.19 Roughness strips

Hongrae Park et al [24]. Studied the varying effect of roughness strips also the Reynold number to note the impact on shear layers while pondered that turbulence is induced in the flow by adding up the roughness due to which the vorticity gets weaker consequently by the diffusion of the vortex. Due to the roughness affecting the amplitude of vibration approaches to negligible values. The shear layer rolls up as well as the vortex shedding gets irregular and sharp changes occur in it. The shear layer becomes chaotic and gets diffused earlier as it is formed. The shear layer does not impart the energy of water to the harvesting flag.

2.20 Impact of roughness on frequency and amplitude

Wang, Jet al. [25] Performed tests in the range of Reynold number $2.5x10^{4}$ – $1.8x10^{5}$ and roughness ranging $1.1x10^{-4}$ – $1.2\ x10^{-2}$. The finding of experimentation shows that the number of participating amplitude and frequencies decreases with an increase in roughness. The onset of lock-in region in the smooth cylinder while in the rough cylinder the lock-in region tends to decrease abruptly.

2.21 Corrosion in seawater

The behavior of Aluminum in seawater was investigated by *Robert E* et al. [26]. The development of pit size and loss of mass was taken into consideration. Over time the aging of Aluminum is either corrosion resistant but the presence of minerals in seawater makes it corrode and erode over time. The immense data for three years was observed from the experimentation. Depth of pit and the loss of mass due to erosion was recorded.

Chapter 3

Methodology

3.1 Experimental layout

The apparatus was installed in the flow visualization lab in the Department of Mechanical and Manufacturing Engineering, School of Mechanical and Manufacturing Engineering (SMME), National University of Sciences and Technology (NUST). An automated water tunnel with a water speed controller was used. Water purified by reverse osmosis was used in the experimentation with a sediments value of less than 25 ppm. The Reynold number (Re)for the experimentation is maintained at Re from 8690 - 9549. The unidirectional flow tunnel is set up by cleaning the honeycomb structure. The water incoming flows into the tunnel by inlet valve. Regularized water flow is maintained at the respective velocity to get stable at a level and speed which is adjusted from the rotational speed of the pump and frequency (f)of the motor. The size and cleanliness of the honeycomb maze are verified to ensure the flow remains laminar.

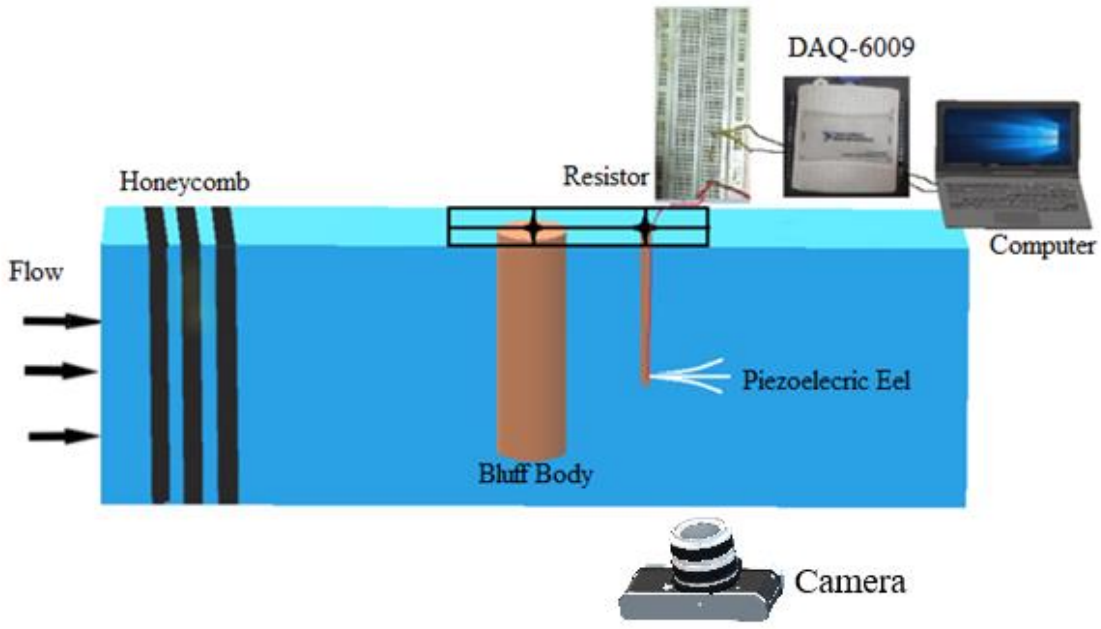

Figure 3.1 Schematic diagram of the experimental setup

The schematic diagram of the apparatus setup is shown in Figure 3.1. Experimentation is carried out on the water tunnel with a velocity U of 0.31 m/s is maintained a pump speed of 25 hertz. The piezoelectric eel is fixed to a thin steel rod of diameter 4 mm, and the rods are fixed

in an aluminum lightweight clamp over the walls of the test section. The piezoelectric eel is placed in a conventional arrangement, clamped at one leading edge and another trailing edge, in uniform flow right after the bluff body.

3.2 Positioning of piezoelectric eel

The streamwise gap Gx and Gy between eel and bluff body is varied through an overhead mounting mechanism. A circular aluminum hollow cylinder is used as a bluff body while the roughness is varied by using suitable sandpaper as shown in Figure 3.1 The roughness of the smooth cylinder is 2.21 microns, and its diameter (D)is 25mm while the second roughness value is 4.07 and its diameter is 27mm, the third cylinder has a roughness of 9.85 diameters of 27.2mm. The last one has a roughness of 13.97 is coarser grit size and has a diameter of 27.5 mm. To incorporate the effect of increasing diameters with different surface roughness, a dimensionless parameter is used in which all four roughness are divided by their respective diameters (K_s/D). Specifications of the parameters utilized in the experimentation are mentioned in figure 3.3.

3.3 Lab Equipment (DAC, HDR camera, optimum, Resistance, Stand, LED)

A high-resolution and high-speed camera of the model (RX100 IV Sony, fixed under the test portion) is utilized to record videos of piezoelectric eels to determine the flapping pattern at 50 frames per second for two minutes. A flashlight is used for the illumination of the test section. Eel is connected to a DAQ card to store the electrical signal data acquired from flapping. The voltage generated from the piezoelectric eel by applying a resistance that is connected between an eel and the DAQ card is measured. The diameter of bluff body ranges from 25 mm to 27.5 mm.

Figure 3.2 Flow Visualization Lab Schematic

3.4 LabVIEW software and optimum Resistance

LabVIEW® software is utilized to visualize the data for further analysis of voltage generated in the waveform obtained also the excel sheet after postprocessing for the same duration as videos which are post-processed for amplitude and frequency in MATLAB. The DAQ card is directly connected to the optimal resistance and that resistance wire is directly connected to PC on which LabVIEW software is operational to visualize the wave form of voltage.

A 1 MΩ resistance is used to calculate the optimal power output by using the maximum power transfer theorem.

$$\text{Power} = V^2/R_{opt}$$

The output is measured against different values of the optimal resistance to validate the similar value of 1MΩ, as shown in Figure 3.1

3.5 MATLAB

The image processing technique is utilized to comprehend the tail position of the flag to evaluate the peak of amplitude (*A/L*) and the Fast Fourier Transform Method (FFT) is taken under consideration to know about the dominant frequency by using MATLAB®. Where frequency and amplitude are plotted, and readable results are visible on the screen of the computer which is different for each case of varying the distance of eel from the bluff body in Gx and Gy as well. To observe the effect of varying the distance on energy harvesting the flapping of eel, frequency, and amplitude of flapping eel were taken into consideration. The wake and vortex of each roughness are visualized which was previously a hypothetic phenomenon while after this experimentation and detailed analysis of 25 cases for each set of roughness, the total of 100 cases effect is studied to deduce a conclusion based on the finding of the researcher of energy harvested.

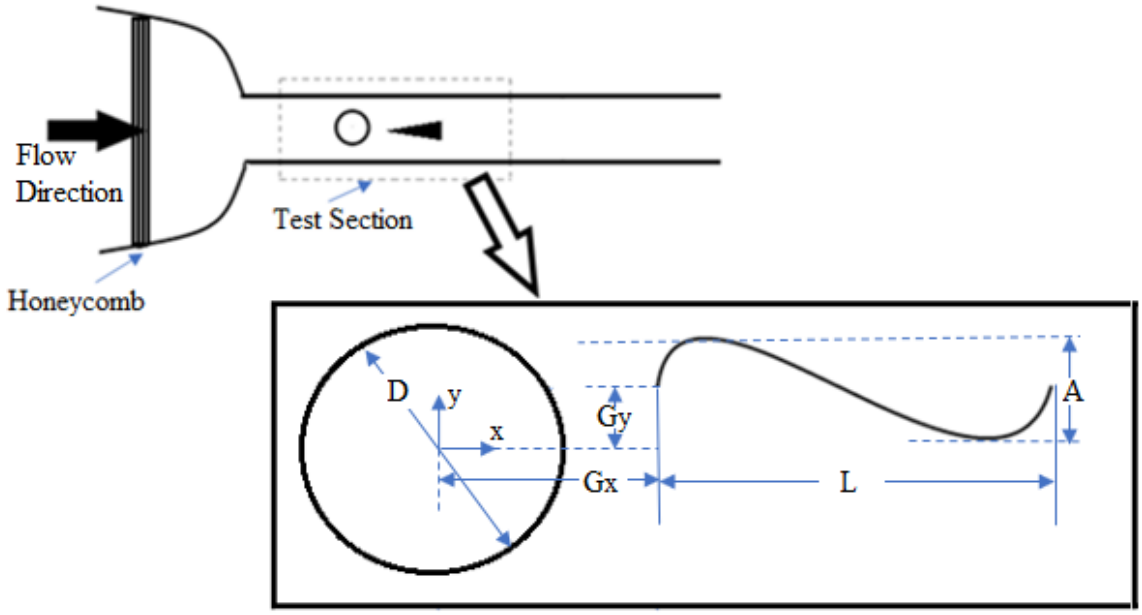

Figure *3.3.* Top View of the Experimental setup

Parameters of Energy harvesting	
Optimal Resistance	1MΩ
Range of Resistance	10kΩ - 2.9 MΩ
Thickness	28µm
Effective length	60mm
Width	12mm
Poison Ratio	0.46
Total length	72mm
Young's modulus	1.38 G-Pa
Density	1.75×10^3 kg/m^3
Voltage generated	0.01-100mV

Figure 3.4 Parameters of PVDF energy harvester

Chapter 4

Results & Discussion

4.1 Varying roughness and Reynolds number

Experiments are performed on a low-speed water tunnel to study the effect of cylinder roughness on the energy harvesting of eel place in the wake of the cylinder. The roughness of the cylinder (K_s/D) of 8.8 $x10^{-5}$, 1.51 x 10^{-4}, 3.62 x $10^{-4,}$ and 5.08 x 10^{-4} is used in the present study. The gap between the center of the cylinder and upstream of eel in x-direction defined as G_x is changed from $1 \leq G_x \leq 3.5$ with an increment of 0.5 for each roughness of the cylinder. Similarly, the gap between the center of the cylinder and upstream of eel in y-direction defined as G_y is changed from $0 \leq G_x \leq 1.5$ with an increment of 0.5 for each roughness of the cylinder. The Reynolds number in the present study is varied from 8690 to 9549. A total of 100 experiments are performed to analyze the effect of surface roughness of the cylinder on energy harvesting from the eel.

4.2 Euler Bernoulli's equation

Figure 4.2 shows the plot of power (P), frequency (f), amplitude (A/L) versus surface roughness at Gx=1.25 and Gy=0 where the maximum energy is harvested for each surface roughness of the cylinder which is referred to as best efficiency power. It is interesting to observe that the best efficiency power decreases with an increase in the surface roughness of the cylinder. The best efficiency power is correlated very well with the amplitude of the eel and its frequency where both the amplitude and frequency increases with power. This is because the deflection of the beam is directly proportional to the strain in the beam according to the Euler Bernoulli equation. The strong vortex shedding from the cylinder exerts a maximum force on the cylinder due to which maximum power is extracted at Gx=1.25 and Gy=0. It is also observed that the maximum power at all the roughness is independent of Gx and Gy as they always occur at Gx=1.25 and Gy=0.

4.3 Results

4.3.1 Roughness verses (Power, Frequency, Amplitude)

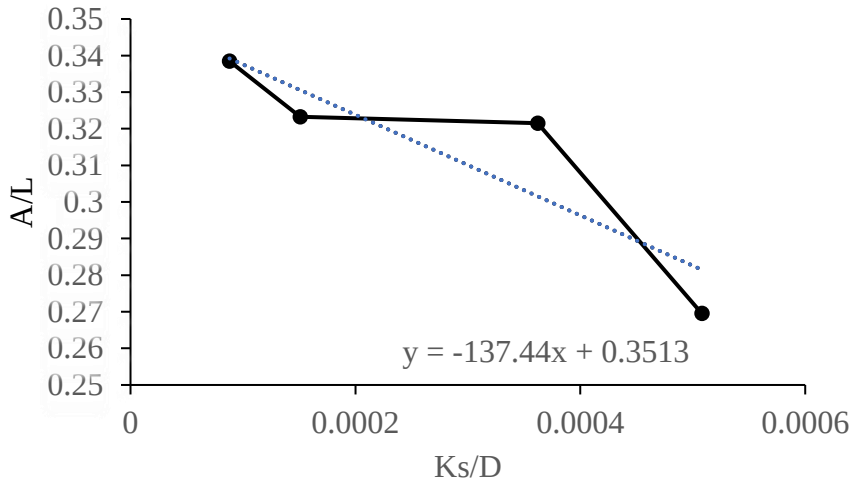

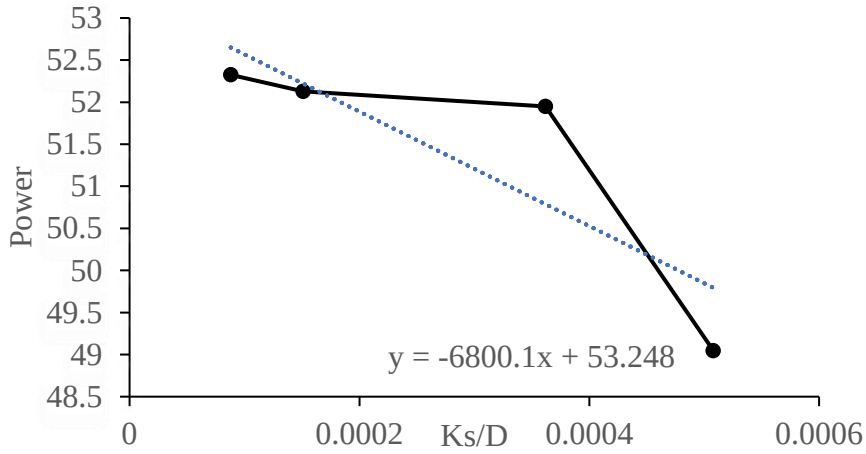

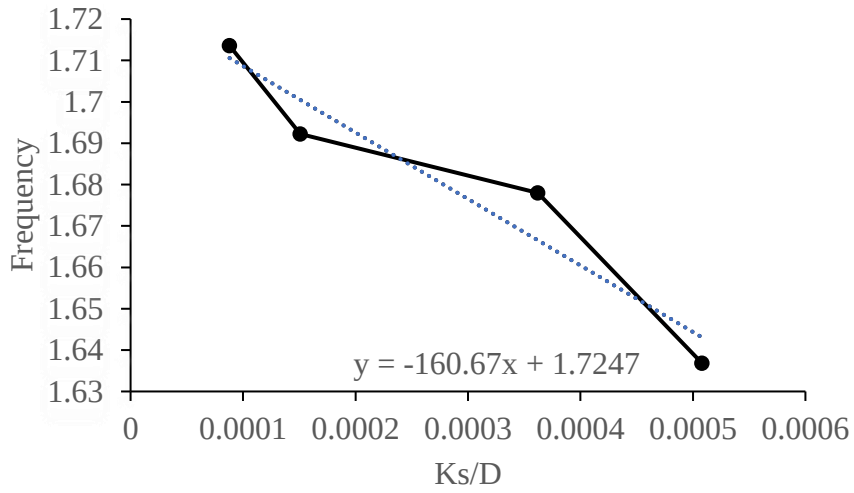

Figure 4.1 Plot of maximum power, amplitude, and frequency of eel versus roughness of the cylinder

4.3.2 Contours of Power(P), Amplitude(A/L), and Frequency(F) in Tecplot

Figure 4.2 shows the contours of Power(P), Amplitude(A/L), and Frequency(f) on a Gx and Gy plane for Ks/D=8.8 $x10^{-5}$ which is very small roughness in sense of grain size and can be approximated as a smooth cylinder. The power, amplitude, and frequency decrease with the increase in both Gx and Gy. The decrease in amplitude is correlated to the vortex shedding in the wake of the cylinder. As the Gx increases, the vortices shed from the cylinder begin to dissipate. This causes the strength of the vortex shedding to decrease and as a result, reduces the force on the eel resulting in a decrease in the amplitude in the x-direction. Likewise, increasing Gy causes the flow to become axis-symmetric upstream of the eel which reduces the force and amplitude consequently. The frequency of the eel also decreases with the increase in Gx and Gy distance , and is directly related to the vortex shedding behind the cylinder. The value of Gx and Gy corresponding to the best efficiency power is also shown in Figure 4.2 a with an asterisk. It occurs at Gx=1.25 and Gy=0. Figure 4.2 is further divided into four regions. The variation of power is strong in the first region I and maximum power are extracted in this region. The energy harvested decreases in the second region II with a further decrease in region III. The minimum power is extracted in region IV.

4.3.3 Maximum and Minimum Flapping and strain in Piezoelectric eel

The first Region mainly describes the extreme power region as optimal lies in the area which is under consideration. The flapping speed of the eel affects the frequency (f) and the strain generated in the eel impacts the amplitude(A/L). So, region one in Gx and Gy direction shows the peak point of maximum energy extraction. The second region mainly moving along the x-axis is depicting the shrinkage of energy (Power) also the flapping speed frequency(f) and strain in the eel which is mainly amplitude (A/L). The contour consists of four different colors. The third region is in the offset distance in the y axis mainly the flapping speed the frequency and the amplitude shrink. The fourth region which is mainly the bluff body is away from the eel so there is a lesser effect of wake on the eel. In the y axis, the offset distance increases in such a way that there is negligible flapping due to which the minimum power is extracted there which is 36.5 microwatt.

4.3.4 Determination of optimal point

The detailed view of the physical appearance of the cylinders an increase in grain size or grit size is taken under consideration so we pondered that the point at which cylinder is just in front of eel at that point maximum flapping is produced because of the maximum shear layer generation from both sides of the bluff body. That area under consideration in which the optimum point lies is determined after the experimentation. The red color of the region near to origin is the verification of max power harvesting at that point while studying this which is gap wise 7 points in the Gx direction and 4 points gap wise difference offset in the Gy direction. While studying the optimum point the experimentation on gap Gx = 1.25 and Gy = 0 is done to ponder on the peak value of Power. The top view of the lab is shown in figure 3.2. The dimensionless distance Gx = S/D where S is the distance from the center of the bluff body to the eel and D is the diameter of the Cylinder.

While moving across the X-axis away from origin the decrement power is visible blue color shows the minimum amount of energy generated by the shear layer generated by the bluff body. The minimum power shown on the plot is 36.4 microwatt while the maximum power on the plot is 52.325 microwatt. The results are discussed in this range so that the fluctuation in the movement is the function of power harvesting. As we move in the Y-axis the Flapping decreases abruptly because the effect of the shear layer on the eel deceases consequently the response of the eel significantly decreases, which can be observed from the decrement of power shown by the different colors the red color shows the maximum power the then lesser one from red is orangish-yellow than yellow after that green color comes and in the last bluish color shows the minimum flapping and reduced energy as a result of surface texture and grain size of the surface is increased so that the physics of shear layer is changed.

The abrupt change in power in the Y direction is due to offsetting in the spanwise gap between the bluff body and the eel increases so large as the impact of the shear layer on the eel goes to be very small having no significant change anymore while the bluish area tends to dominate in the roughness of 13.97 microns.

4.4 For $K_s/D = 8.8 \times 10^{-5}$

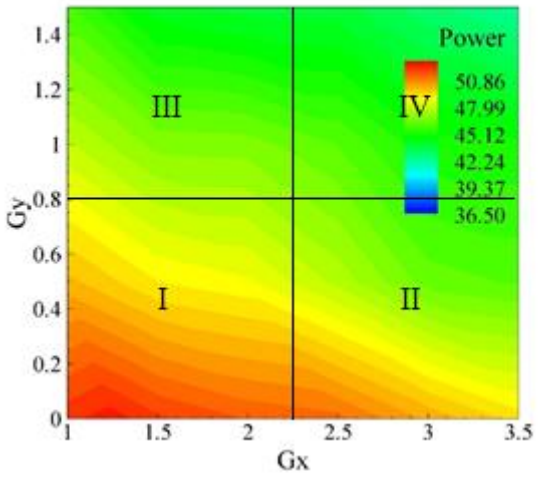

(a)

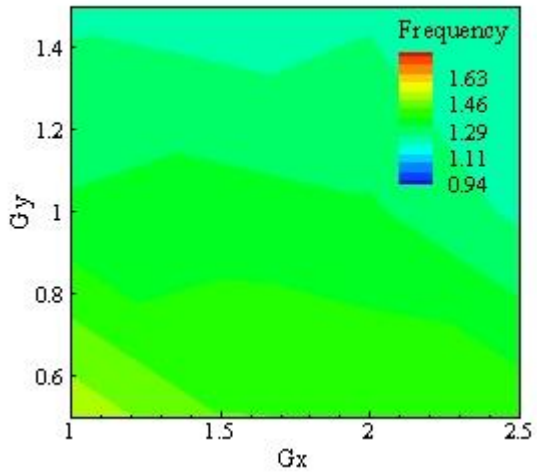

(b)

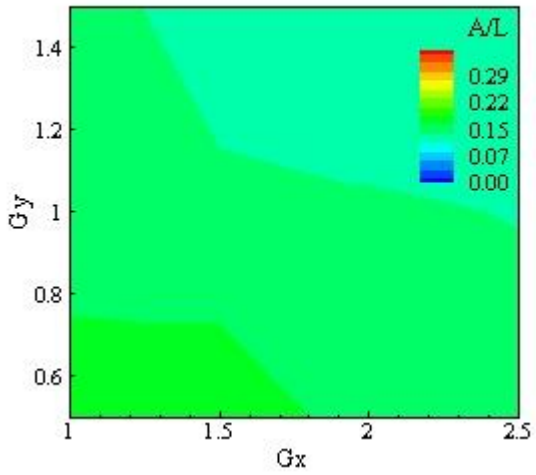

(c)

Figure 4.2 Results for $K_s/D = 0.88 \times 10^{-4}$, (a) Power, (b) Amplitude, and (c) Frequency

The detailed investigation of results obtained from the different dimensionless roughness factors which are used in the experimentation artificially designed range of roughness, to depict the results of corrosion pitting on the aluminum cylinder for aging. During the process of aging chemical reaction occurs also by the flow of salty water of subsea containing Na+ and Cl- ions tend to corrode and remove the upper layer of material with flow direction The upper layer gets weaker finally removed and hollow pits get visible and the surface is eroded resultantly.

Currently, the pits in sense of roughness are co-related to the energy gaining which becomes less efficient due to lack of smoothness the passage of flow is disturbed consequently, the wake

region gets narrower as we increase the roughness. Figure 4.2 (a, b, c) plots respectively show the result of Power, Amplitude, and Frequency. The power is maximum at the Gx =1.25 and Gy =0 the shear layer formed from the bluff body wake in both ways of the bluff body is maximum at that point merge in such a way that flapping area is maximum as well the flapping frequency is also more due to which max power is gained. As shown in Figure 4.2. The experimental data (Gx, Gy, Power) is triangulated in the Tec plot which does not shows the exact optimal point in the experimental data.. For precision, an excel sheet is provided to study the results.

4.5 For $K_s/d = 1.51 \times 10^{-4}$

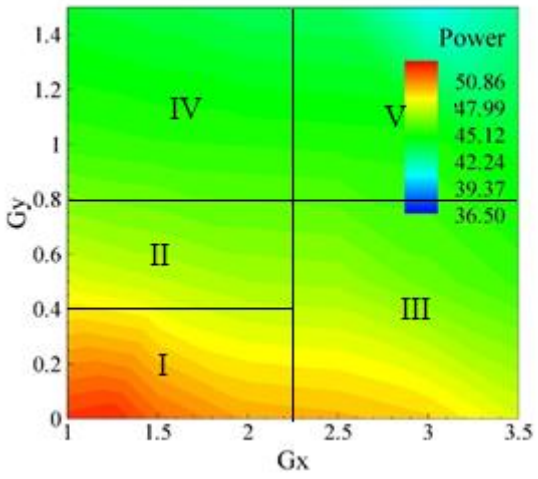

(a)

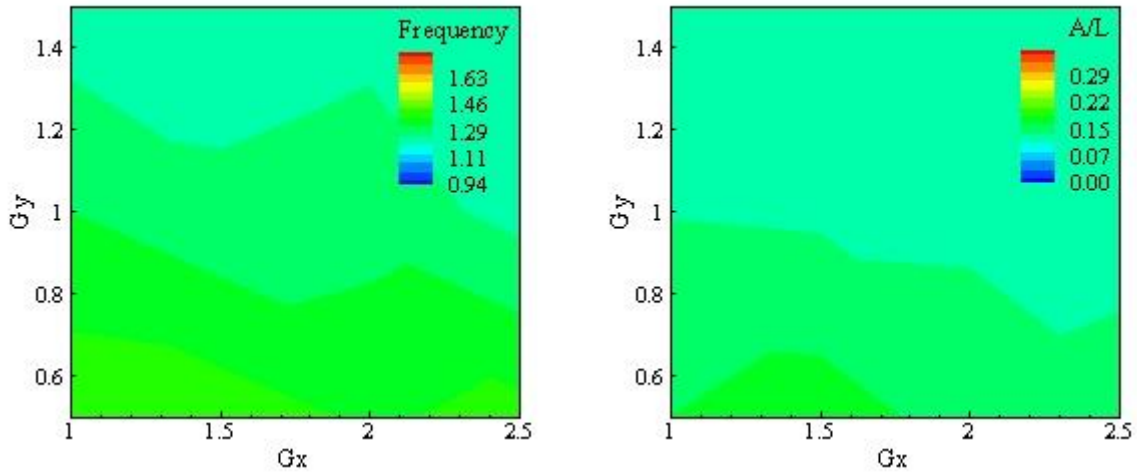

(b) **(c)**

Figure 4.3 Results for $K_s/D = 1.51 \times 10^{-4}$, (a) Power, (b) Amplitude, and (c) Frequency

Following the effect of aging on the surface of the cylinder the roughness pitting of the cylinder tends to increase as a result the efficiency to provide energy as a bluff body also decreases. The power is maximum at the Gx =1.25 and Gy =0 the shear layer formed from the bluff body wake in both ways of the bluff body is maximum at that point merge in such a way that flapping area is maximum as well the flapping frequency is also more due to which max power is gained the power contour is split into five subsections. In the subsection, the power gained is the most. in the first subsection in Gy from 0 to 0.2 while in Gx from 1 to 2.25 in which the maximum flapping owes the maximum frequency(f) and maximum amplitude(A/L) which tends to raise the power of the subsection. The second subsection graphs ranging from 0.4 to 0.8 in Gy and

Gx is 1 to 2.25 which is lesser in Power harvesting from the 1st subsection. The third subsection is from 2.25 to 3.5 in Gx and 0 to 0.8 in the Gy direction having the same energy as the second subsection. 4^{th} subsection has green color depicting the reduction of power(P), frequency(f), and amplitude(A/L). While the fifth subsection is the least power extracting region because the speed of the flap as well as the displacement of the flap is very small so that the product of frequency (f) and amplitude (A/L) will be least. This is depicted from the test the roughness is enhanced to 1.51×10^{-4} so that the peak area of energy decreases because of lesser flapping of eel in that area as the gap of Gx and Gy is varied in a constant manner of 0.5 mm. As in x-direction, the eel is moved away from the origin the spanwise gap from the bluff body increases as a result the impact of vortex energy being evolved from the bluff body wake is not able to reach the level it was formerly reaching so the flapping tends to lessen and the power becomes lesser. The optimum value of power in Gx and Gy is (1.25,0). As shown in figure 4.3. Tec plot provides the necessary contour for the given experimental data shows the trend of the data provided in this scheme the triangulation of data is done at the spanwise gap of 0.5. For the elaboration of optimum points excel graphs are also plotted below to ponder the optimal points respectively.

4.6 For $K_s/d = 3.62 \times 10^{-4}$

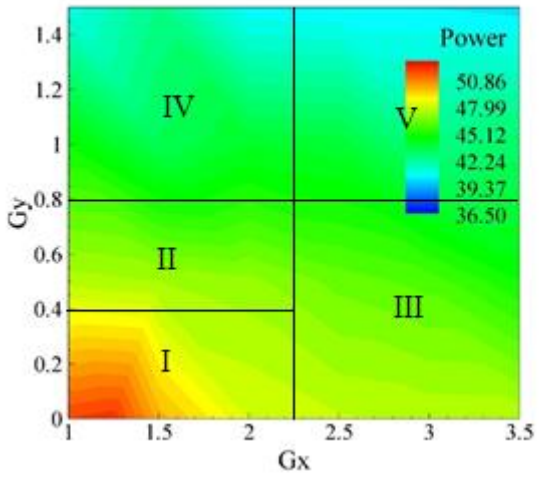

(a)

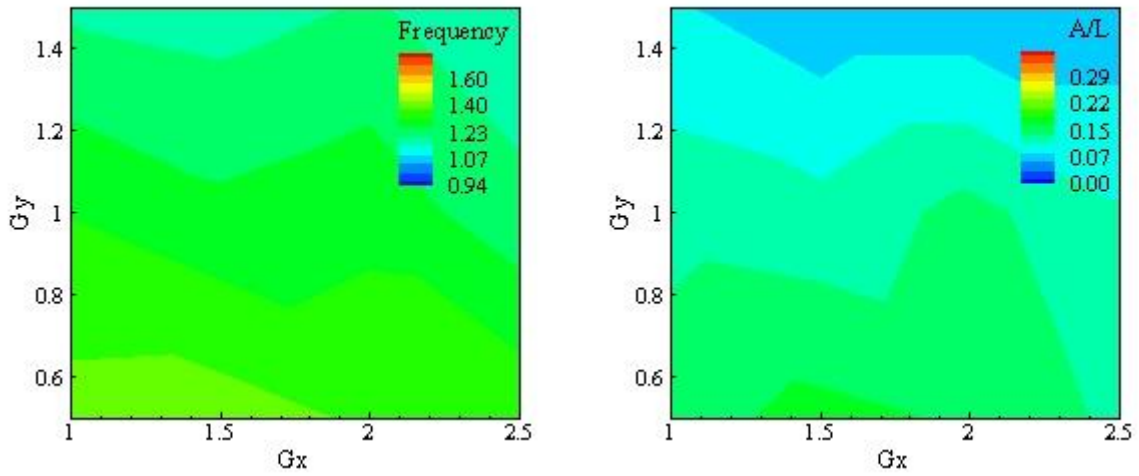

(b) (c)

Figure 4.4 Results for $K_s/D = 3.62 \times 10^{-4}$, (a) Power, (b) Amplitude, and (c) Frequency

In this case, Figure 4.4 (a, b, c) plots respectively show the result of Power, Amplitude, and Frequency. The power is maximum at the Gx =1.25 and Gy =0 the shear layer formed from the bluff body wake in both ways of the bluff body is maximum at that point merge in such a way that flapping area is maximum as well the flapping frequency is also more due to which max power is gained the power contour is split into five subsections. In the subsection, the power gained is the most. in the first subsection in Gy from 0 to 0.2 while in Gx from 1 to 2.25 in which the maximum flapping owes the maximum frequency(f) and maximum amplitude(A/L) which tends to raise the power of the subsection. The second subsection graphs ranging from 0.4 to 0.8 in Gy and Gx is 1 to 2.25 which is lesser in Power harvesting from the 1st subsection. The third subsection is from 2.25 to 3.5 in Gx and 0 to 0.8 in the Gy direction having the same energy as the second subsection. The 4th and 5th subsections have bluish-green colors depicting the reduction of power (P), frequency(f), and amplitude(A/L). The reddish color shows the max power of approximately 52.325 microwatts while 36.4 microwatt is the minimum power harvested in our cases is shown in dark blue. Point (1,0) is taken as a reference or origin to the span-wise gap in Gx and Gy direction. The optimum location of power in Gx and Gy is (1.25,0). shown in Figure 4.4. As the Tecplot provides the contour for the experimental data, the given data is triangulated spanwise.

4.7 For $K_s/d = 5.08x\ 10^{-4}$

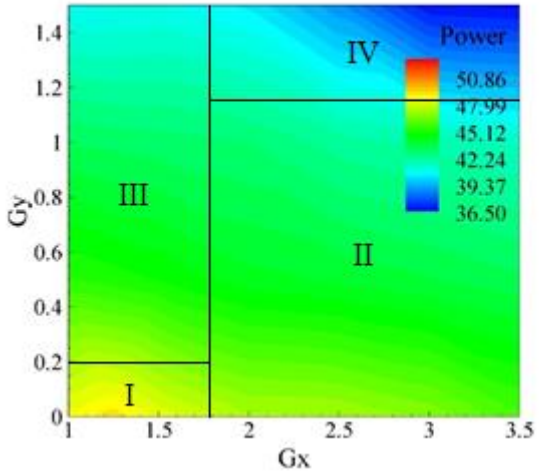

(a)

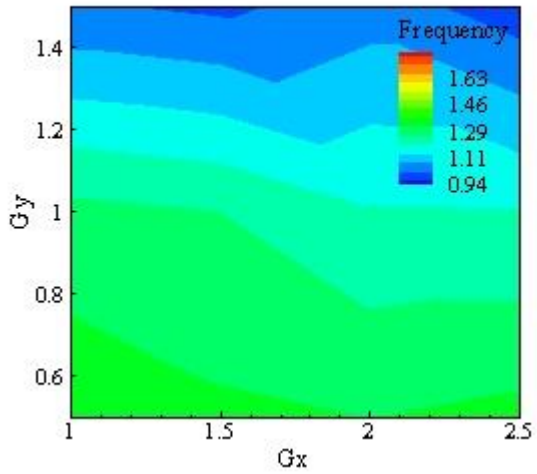

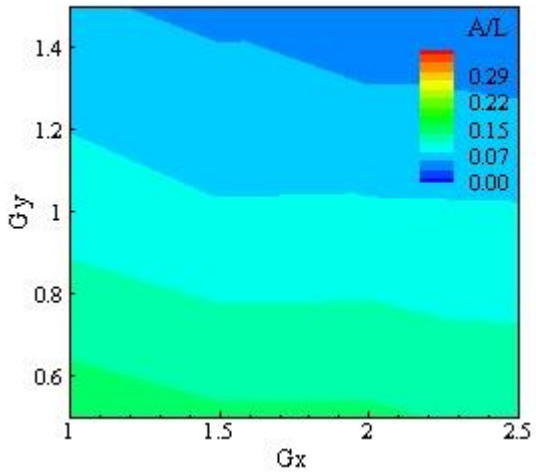

(b) (c)

Figure 4.5 Results for $K_s/D = 508\ x10^{-6}$, (a) Power, (b) Amplitude, and (c) Frequency

In figure 4.5 the contour is divided into four sub-sections to study and differentiate between the maximum Power position of the eel as the optimum point. Subsection 1 is containing the Power more than the other three sections while the second subsection relatively contains less power from the previous, the third region has the same energy harvesting as subsection 2 And the 4th Subsection has the least Power because the power (P) is dependent on the frequency and amplitude of flapping eel. The speed of flapping eel is thereby, affects the frequency the

most while the maximum displacement of the free end of the eel tends to affect the Amplitude (A/L) of the eel. As in this case, the maximum surface roughness is used and kept at a position where the stimuli of the wake of flow around the circular cylinder bluff body don't affect the eel flap or have a very minute effect on the flap of the eel so due to which a poor flapping or negligible flapping is observed. The deep observance of plots of 5.08 x 10^{-4} shows that the power, frequency, and amplitude are minimum in the whole plot as greenish and bluish color is dominant in the graph. A small region with orange and yellow color is visible near the origin at (1,0). The optimum power location in Gx and Gy direction is found as (1.25,0). The region away from the optimum point shown in blue color is low energy region observing by the experimentation the impact of flapping eel is low there almost flapping is negligible also the amplitude is much decreased from the optimal point values. The least amount of energy is depicted on the bluish region the point is (3,1.5) and the second minimum energy point is (3.5,1.5). As shown in figure 4.5.

4.8 For Graph max power output

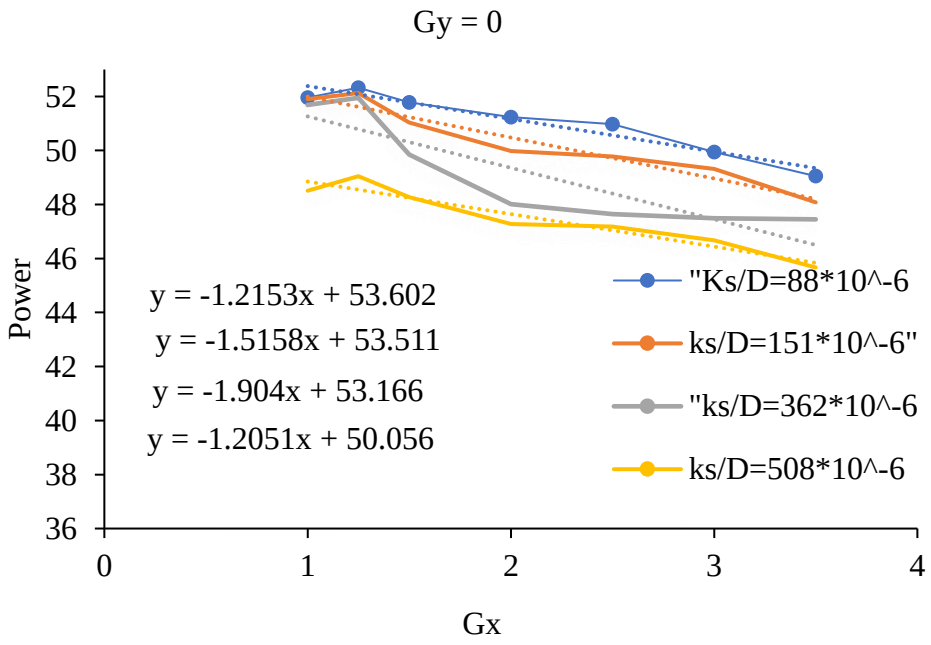

Figure 4.6 Graph For max Power at Gy=0

The elaboration of max power harvested at Gy=0 while the Gx gap is 1.25 which is found to be the optimal point for the energy harvested from the cylinder having roughness varying from maximum to minimum range as provided in the experimentation. The dimensionless roughness factor which different for each case. The shear layer gets narrower as the roughness factor

increase because the energy dissipates earlier as the roughness factor increases. All the phenomena are depicted in the plot. The dissipation of the shear layer and its effectiveness also gets low.

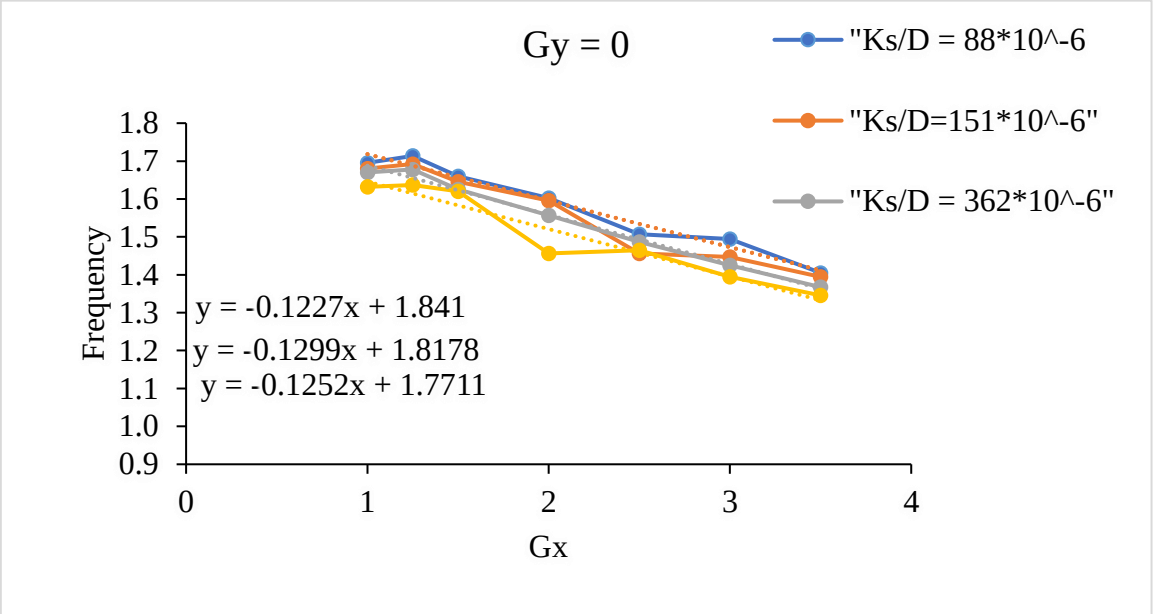

Figure 4.7 Graph for max frequency at G y=0

The graph of frequency is shown which is plotted to show the maximum frequency obtained. The optimum point is marked as (1.25,0). Frequency is maximum for the smooth bluff body also at a point near to the bluff body. Moving away in Gx and Gy the response off eel will get lesser due to dissipation of shear layer. In Figure 4.7.

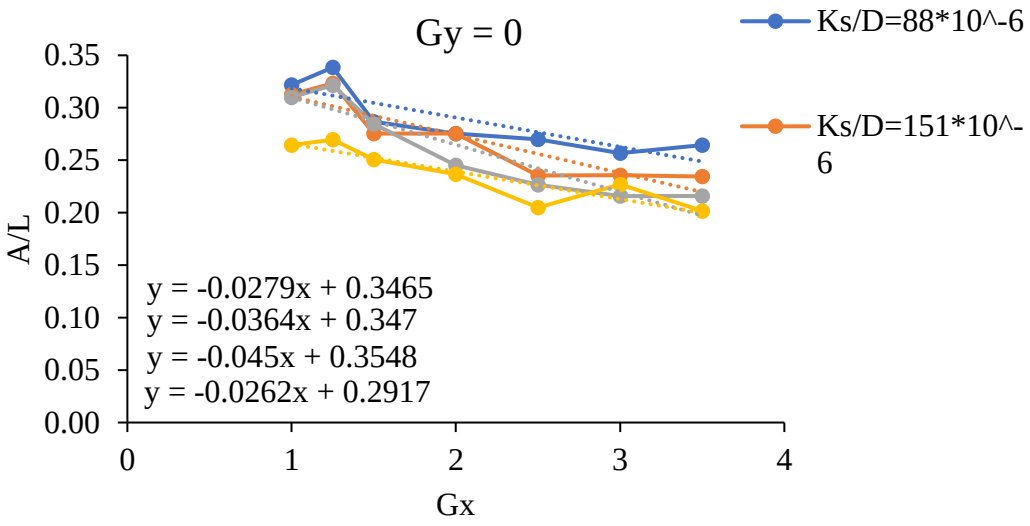

Figure 4.8 Graph for Max Amplitude/Length at Gy=0

The A/L ratio of the flapping eel is dependent on the surface roughness and the optimal point on which maximum power and frequency are located so amplitude and frequency of flapping finally make the resultant power harvested. At point (1.25,0) maximum amplitude is observed is plotted in this graph figure 4.8.

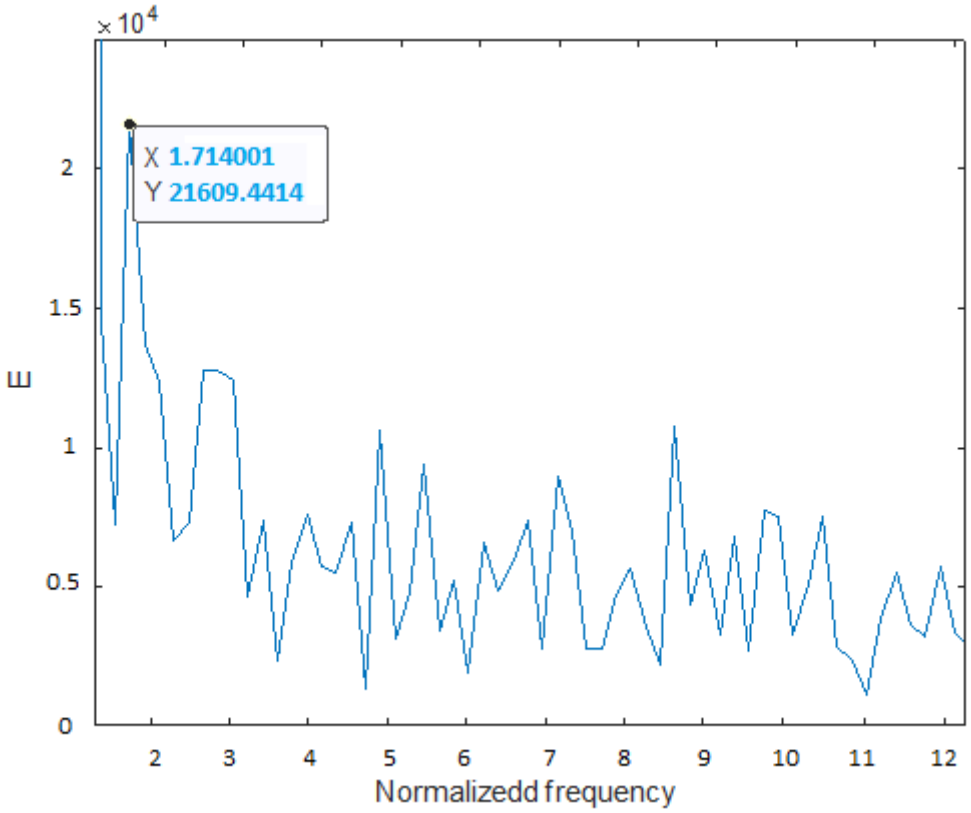

Figure 4.9 Frequency Chart for optimal maxima case (Frequency= 1.714)

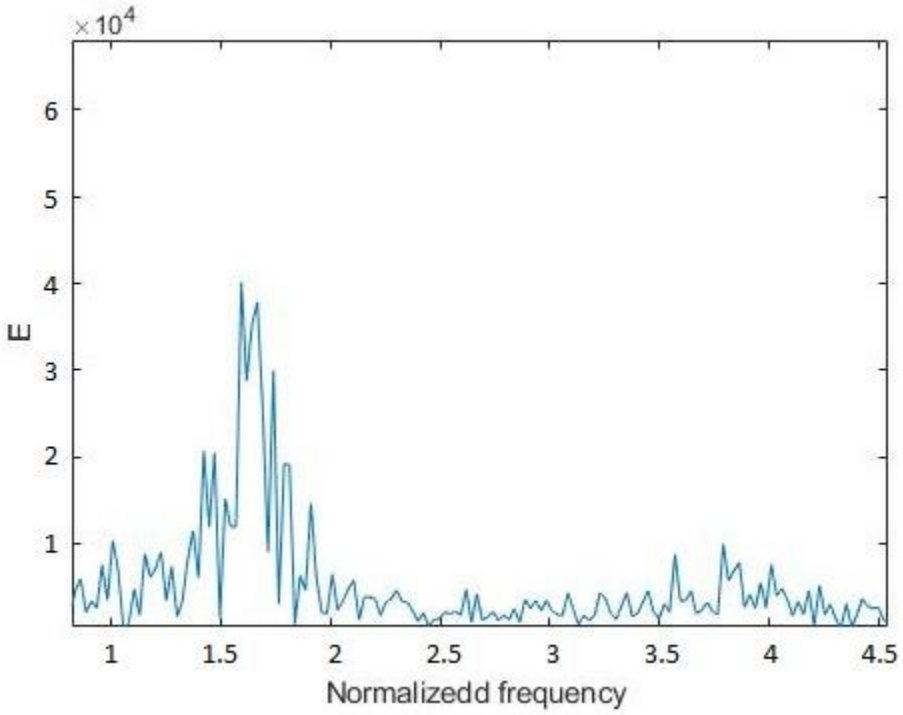

Figure 4.10 Frequency Chart for second optimal maxima case (Frequency= 1.692)

The maximum Normalized frequency is observed for the cylinder having a roughness of 8.8 $x10^{-5}$ shown in figure 4.9 at the point of experimentation (1.25,0) having the optimal point at (1.25,0) which is 1.714. The second highest normalized frequency at the cylinder with the roughness of 151 microns is shown in the figure at (1.25,0) The normalized frequency is 1.692

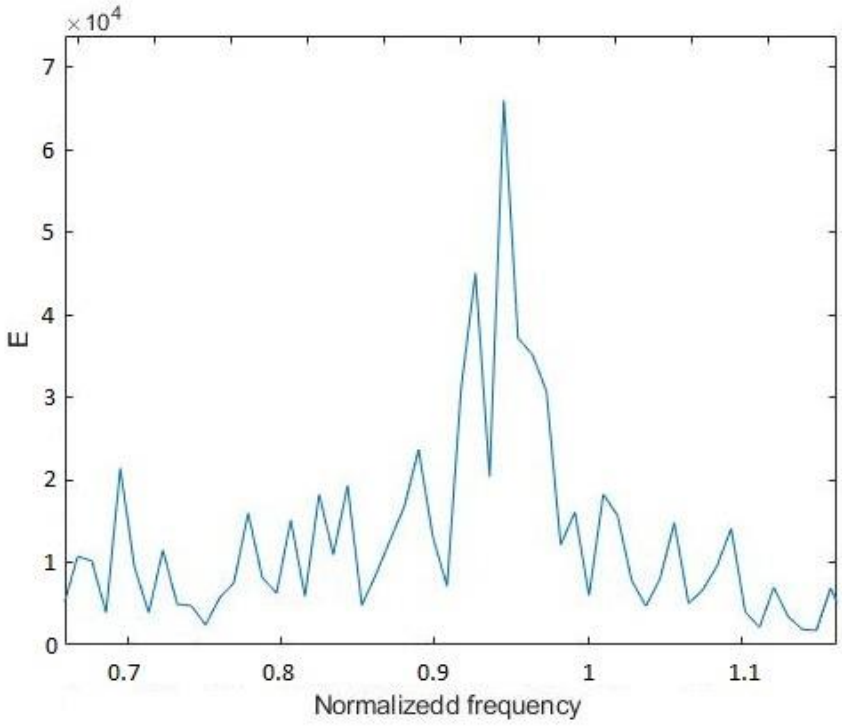

Figure 4.11 Frequency Chart for optimal minima case (Frequency= 0.946)

4.9 Bifurcation frequency in eel.

Bifurcation phenomena occur in the frequency which is mainly due to the dual-frequency of eel. Sometimes eel operates at two frequencies because, in a water tunnel, there occurs frequency fluctuation due to the instability of the water of the tunnel. The phenomena mainly occur in the water tunnel due to chaotic flow in the tunnel while somehow after achieving the stability the bifurcation is limited and controlled up to some extent. In this eel, the thickness is 28 micrometers there occurs the fluttering in the eel also due to the increase in speed of flow or increasing the Reynold number from some critical value.

4.10 Minimum Value for Frequency

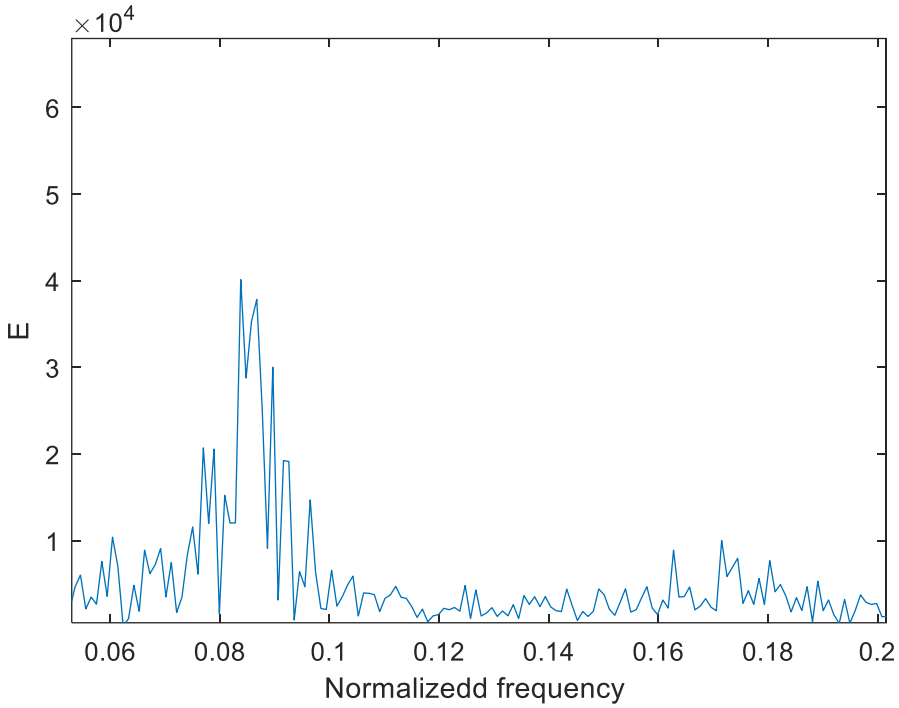

Figure 4.12 Frequency Chart for second optimal minima case (Frequency= 0.957)

The minimum values for normalized frequencies are shown in figure 4.11 and figure 4.12. The minimum values are at the point (3.5,1.5) and (3,1.5) The minimum frequencies are 0.946 and 0.957. The minimum frequency means at that point the flapping speed of eel is very low or approaches a very small value so taking that point as the least point of frequency. As the frequency is co-related to the flapping speed.

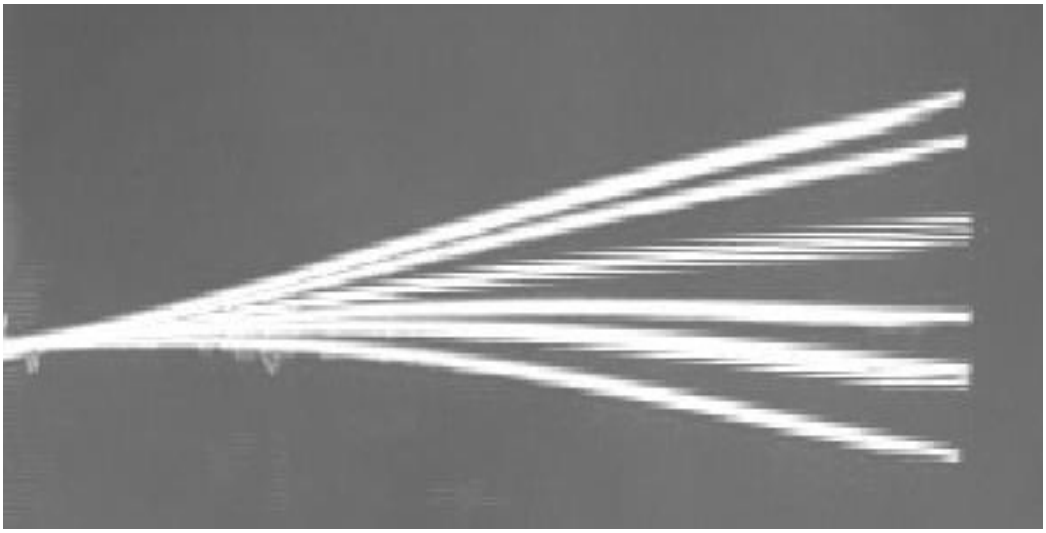

Figure 4.13 Stroboscopic image for amplitude of A/L=0.338

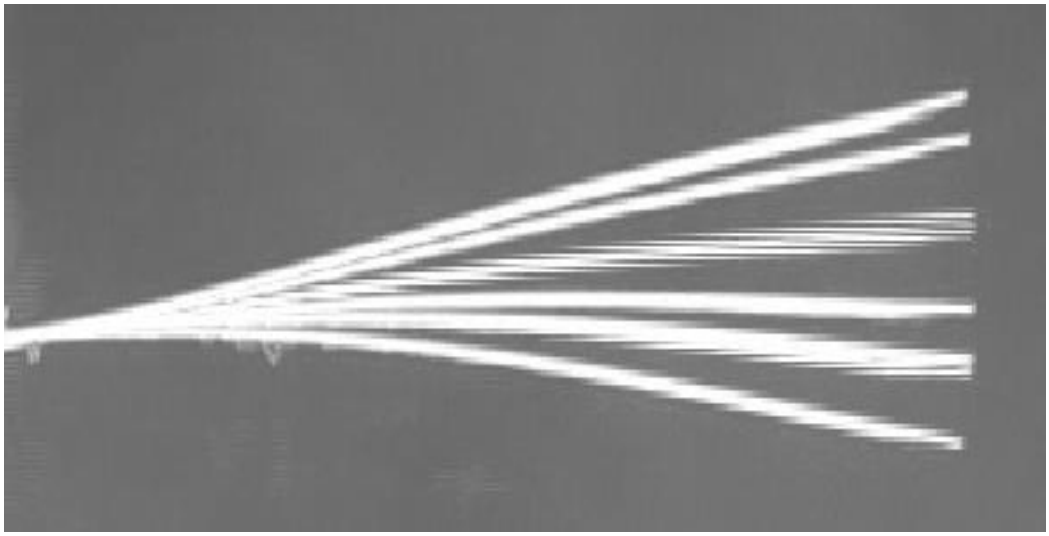

Figure 4.14 Stroboscopic image for amplitude of A/L=0.323

Figure 4.15 Stroboscopic image for amplitude of A/L= 0.028

Figure 4.16 Stroboscopic image for amplitude of A/L= 0.02

The dependence of amplitude is mainly on the strain produced in the eel. The more is deformation or strain is generated in the eel the more amplitude will be observed in the eel. The smooth cylinder has the maximum strain and amplitude as well at Gx 1.25 while the lowest amplitude is observed at 3.5 for the rough cylinder of roughnes13.97. Figure 4.13 depicts the maximum amplitude produced in the piezoelectric eel when it is placed in the direction of at the optimum distance from the bluff body at a position where maximum strain is produced in the piezoelectric eel.

Non-dimensionalized Roughness (Ks/D)	Power(**P**) Reduction (%)	Frequency(f) Reduction(%)	Amplitude(A/L) Reduction(%)
$8.84x\ 10^{-5}$	52.325 µW	1.695545	0.32176
(Without sandpaper)	(Reference)	(Reference)	(Reference)
$1.507\ x\ 10^{-4}$	1.346	1.182	5.955
$3.621\ x\ 10^{-4}$	3.462	2.416	11.561
$5.08\ x\ 10^{-4}$	6.26	4.5	20

Figure 4.17 Annotation of Results

The experimentation was done by A Mujtaba et al. [27] In the same lab. Has performed the experimentation for energy harvesting for naked cylinder and tandem position of two flags. The validation of results in this research is comparable to this research. The conditions and parameters are different while and equipment are the same. The eel used by A Mujtaba et al is 52 micrometers thick while used in this research is 28 micrometers. The velocity of water circulation in the water tunnel is variable while in this research water speed is 0.31m/s. The same flow visualization lab is used for multiple experimentations earlier by the researchers and multiple results are deduced from the outcome of the experimentations.

Chapter 5

Conclusion and Future work

5.1 Conclusion

Over time, Pits develop on the surface of the aluminum cylinder, the surface corrosion increases with an increase in pit size. Experimentally verifying the impact of aging as a function of surface roughness. All four different roughness of cylinders is verified with the increase in surface roughness of the cylinder the energy harvesting, which is dependent on power, is the function of the speed of flapping (frequency of eel) and area covered during flapping (amplitude). The power is maximum at the position of the eel. Fixing the eel at different gaps with a fixed gap of 0.5 while the cylinder is fixed, we conclude at a point that power, flapping frequency, and amplitude are maximum at the point is varying for each roughness taken into consideration. Experimentation is done at a span gap of (1.25,0) the optimal point is located approximately at 1.25 span gap. The maximum power was harvested for the cylinder with the roughness of 88 x 10^{-6} is noted as 52.325 microwatts at the position of (1.25,0) while the minimum power harvested for the roughness value of 508*10^{-6} is noted as 36.4 microwatts. The overall 20% reduction in amplitude,6.26 % reduction in power, and 4.5% reduction in flapping frequency are noticed by the aging of the bluff body.

5.2 Future Work

In the upcoming future, the Impact of aging should be thoroughly studied in VIV response. In this research, the experimental work is limited up to MATLAB and LabVIEW software. The voltage signal is generated from the piezoelectric eel and post-processing of videos from the HDR camera. Moreover, a detailed view of the vortex should be undertaken in vortex-induced vibration. In this scheme, the wake of the bluff body is fully visual to study the behavior of contour and the vortex generated by the variation of the roughness of bluff and changing the spanwise as well. The shear layers are visible to deduce the results.

References

[1] Leland, E. S., & Wright, P. K. (2006). Resonance tuning of piezoelectric vibration energy scavenging generators using compressive axial preload. *Smart Materials and Structures*, *15*(5), 1413.

[2] Kamenar, E., Zelenika, S., Blažević, D., & Šamanić, I. River flow energy harvesting by employing piezoelectric eels. In *Proc. 14th EUSPEN International Conference* (Vol. 1, pp. 63-66).

[3] Xie[1], J. M., & Hu[1], Y. T. (2015, May). A circular-cylinder piezoelectric energy harvester based on flow-induced flexural vibration mode and its nonlinear characteristics near resonance. In *The 6th International Conference on Computational Methods (ICCM2015)*.

[4] Williams, C. B., & Yates, R. B. (1996). Analysis of a micro-electric generator for microsystems. *sensors and actuators A: Physical*, *52*(1-3), 8-11.

[5] Wang, Q., & Wu, N. (2011). A review on structural enhancement and repair using piezoelectric materials and shape memory alloys. *Smart Materials and Structures*, *21*(1), 013001.

[6] Rocha, J. G., Goncalves, L. M., Rocha, P. F., Silva, M. P., & Lanceros-Mendez, S. (2009). Energy harvesting from piezoelectric materials is fully integrated into footwear. *IEEE transactions on industrial electronics*, *57*(3), 813-819.

[7] Simpson, R. L. (1981). A review of some phenomena in turbulent flow separation.

[8] Allen, J. J., & Smits, A. J. (2001). Energy harvesting eel. *Journal of fluids and structures*, *15*(3-4), 629-640.

[9] Latif, U., Uddin, E., Abdullah, C., Ali, Z., Sajid, M., Akhtar, K., & Shah, S. R. (2020). Experimental investigation of energy harvesting behind a bluff body. *Journal of Renewable and Sustainable Energy*, *12*(3), 033301.

[10] Latif, U., Uddin, E., Younis, M. Y., Aslam, J., Ali, Z., Sajid, M., & Abdelkefi, A. (2021). Experimental electro-hydrodynamic investigation of flag-based energy harvesting in the wake of inverted C-shape cylinder. *Energy*, *215*, 119195.

[11] Ding, L., Zhang, L., Wu, C., Mao, X., & Jiang, D. (2015). Flow-induced motion and energy harvesting of bluff bodies with different cross sections. *Energy Conversion and Management*, *91*, 416-426.

[12] Allen, D. W., & Henning, D. L. (2001, April). Surface roughness effects on vortex-induced vibration of cylindrical structures at critical and supercritical Reynolds numbers. In *Offshore Technology Conference*. One Petro.

[13] Bernitsas, M. M., Raghavan, K., & Duchene, G. (2008, January). Induced separation and vorticity using roughness in VIV of circular cylinders at 8× 103< Re< 2.0× 105. In *International Conference on Offshore Mechanics and Arctic Engineering* (Vol. 48227, pp. 993-999).

[14] Gao, Y., Zhong, Z., Zou, L., & Jiang, Z. (2018). Effect of surface roughness on vortex-induced vibration response of a circular cylinder. *Ships and Offshore Structures*, *13*(1), 28-42.

[15] Han, Xiangxi,et al. "Surface roughness effect on cylinder vortex-induced vibration at moderate Re regimes." *Ocean Engineering* 224 (2021): 108690.

[16] Ghazali, Mohd Kushairi Mohd,et al. "Surface Roughness Effect on Vortex-Induced Vibration Phenomenon in Cross-Flow Direction of a Bluff Body." *Journal of Advanced Research in Fluid Mechanics and Thermal Sciences* 64.2 (2019): 253-263.

[17] Ramzi, N. A. S.,et al. "Experimental analysis on vortex-induced vibration of a rigid cylinder with different surface roughness." *IOP Conference Series: Materials Science and Engineering*. Vol. 469. No. 1. IOP Publishing, 2019.

[18] Okajima A, Nagamori T, Matsunaga F, Kiwata T. 1999. Some experiments on flow-induced vibration of a circular cylinder with surface roughness. J Fluids Struct. 13:853–864.

[19] Kiu KY, Stappenbelt B, Thiagarajan KP. 2011. Effects of uniform surface roughness on vortex induced vibration of towed vertical cylinders. J Sound Vib. 330:4753−4763.

[20] Allen DW, Henning DL. 2001. Surface roughness effects on vortex-induced vibration of cylindrical structures at critical and supercritical Reynolds numbers. Proceedings of the Offshore Technology Conference; 2001 Apr 30−May 3; Houston, Texas, USA.

[21] Bernitsas MM, Raghavan K, Duchene G. 2008. Induced separation and vorticity using roughness in VIV of circular cylinders at 8 × 103 < Re < 2.0 × 105. Proceedings of the Offshore Mechanics and Arctic Engineering Conference; 2008 June 15–20; Estoril, Portugal.

[22] Kiu KY, Stappenbelt B, Thiagarajan KP. 2011. Effects of uniform surface roughness on vortex-induced vibration of towed vertical cylinders. J Sound Vib. 330:4753−4763.

[23] Gao Y, Fu S,Wang J, Song L, Chen Y. 2015. Experimental study of the effects of surface roughness on the vortex-induced vibration response of a flexible cylinder. Ocean Eng. 103:40–54.

[24] Park, Hongrae, Michael M. Bernitsas, and R. Ajith Kumar. "Selective roughness in the boundary layer to suppress flow-induced motions of a circular cylinder at 30,000< Re< 120,000." Journal of offshore mechanics and Arctic engineering 134.4 (2012).

[25] Gao Y, Fu S,Wang J, Song L, Chen Y. 2015. Experimental study of the effects of surface roughness on the vortex-induced vibration response of a flexible cylinder. Ocean Eng. 103:40–54

[26] Melchers, Robert E. "Time dependent development of aluminium pitting corrosion." Advances in Materials Science and Engineering 2015 (2015).

[27] Mujtaba, A., Latif, U., Uddin, E., Younis, M. Y., Sajid, M., Ali, Z., & Abdelkefi, A. (2021). Hydrodynamic energy harvesting analysis of two piezoelectric tandem flags under influence of upstream body's wakes. Applied Energy, 282, 116173.

[28] Bearman, P. (2011). "Circular cylinder wakes and vortex-induced vibrations." Journal of Fluids and Structures 27(5-6): 648-658.

[29] Kwon, S.-D. (2010). "A T-shaped piezoelectric cantilever for fluid energy harvesting." Applied physics letters 97(16): 164102.

[30] Latif, U., et al. (2021). "Experimental electro-hydrodynamic investigation of flag-based energy harvesting in the wake of inverted C-shape cylinder." Energy 215: 119195.

[31] Sessler, G. (1981). "Piezoelectricity in polyvinylidenefluoride." The Journal of the Acoustical Society of America 70(6): 1596-1608.

[32] Shi, S., et al. (2013). "Flapping dynamics of a low aspect-ratio energy-harvesting membrane immersed in a square cylinder wake." Experimental Thermal and Fluid Science 46: 151-161.

[33] Uddin, E., et al. (2013). "Interaction modes of multiple flexible flags in a uniform flow." Journal of Fluid Mechanics 729: 563-583.